Thermal emission properties of one-dimensional grating with different parameters*

Weixin Lin(林伟新)[1], Guozhou Li(李国洲)[1], Qiang Li(李强)[2], Hongjin Hu(胡宏锦)[1], Fang Han(韩防)[1], Fanwei Zhang(张樊伟)[1], and Lijun Wu(吴立军)[1,†]

[1] *Guangdong Provincial Key Laboratory of Nanophotonic Functional Materials and Devics, School of Information and Optoelectronic Science and Engineering, South China Normal University, Guangzhou* 510006, *China*

[2] *Department of Physics, Hong Kong University of Science and Technology, Clear Water Bay, Kowloon, Hong Kong, China*

(Received 7 November 2016; revised manuscript received 16 December 2016; published online 30 March 2017)

Thermal emission is often presented as a typical incoherent process. Incorporating periodic structures on the tungsten surface offers the possibility to obtain coherent thermal emission sources. Here we illustrate grating as an example to examine the influence of the geometric parameters on the thermal emission properties. It is found that for very shallow gratings, only surface plasmon polariton (SPP) modes can be excited and the emission efficiency is closely related with the filling factor. When the ratio of the depth to period of the grating is in the range from 1/20 to 1/2, the field between the adjacent corners can be coupled to each other across the air gap for the filling factor larger than 0.5 and produce a similar resonance as in an air rod. Further increase of the grating depth can cause the groove of the grating forming metal–insulator–metal (MIM) structures and induce surface plasmon standing wave modes. Our investigations will not only be helpful for manipulating thermal emission properties according to applications, but also help us understand the coupling mechanism between the incident electromagnetism waves and gratings with different parameters in various research fields.

Keywords: surface plasmon polaritons, thermal emission, grating, surface plasmon standing wave

PACS: 73.20.Mf, 44.40.+a, 41.50.+h **DOI:** 10.1088/1674-1056/26/5/057301

1. Introduction

Due to their unique properties to confine light in an extremely small area and potential applications in various fields of nanometer science and technology, surface plasmon polaritions (SPPs) have attracted tremendous interests in these last few decades.[1–5] They cannot be excited directly by incident electromagnetic waves on flat metal surfaces because of the momentum mismatch between the incident waves and SPPs. To compensate the momentum, a prism, a grating, or a defect is required on the metal surface. Utilizing a grating to afford an extra wavevector to compensate the momentum is one of the most widely applied methods.[6]

In contrast to lasing,[7,8] thermal emission is a typical incoherent process.[9] Obtaining controllable thermal emitting sources in the midinfrared spectrum range has been one of the important tasks in photonics technology.[10] When very shallow grating structures are introduced into the metal surfaces, spatially and temporally coherent thermal emission sources can be realized by exciting SPPs.[11–13] For example, we have proposed a two-dimensional orthogonally crossed shallow grating to produce an orthogonally-polarized dual wavelength radiation from a tungsten thermal source.[14] On the other hand, if we incorporate very deep gratings into the metal surfaces, microcavity modes can be excited and coherent thermal emission sources can be obtained.[15–18] In most of the related research, however, only very shallow (the height h being less than a twentieth of the period a) or very deep gratings ($h/a > 1/2$) are utilized to control the thermal emission. There is actually a large gap between them which affects the emission properties significantly. Furthermore, the influence of the grating's filling factor is entangled with its depth. Therefore, appropriate geometrical parameters of the incorporated grating have to be chosen cautiously according to the application fields. Surprisingly, there are very few papers examining the influence of the geometrical parameters (in a large range) on the emission properties of the grating structures.

In this paper, we investigate the evolution process of the emission properties with the filling factor and the depth of the tungsten gratings. It is found that the influence of the depth and the filling factor is correlated as they are changed. When the ratio between the depth and the period is less than 1/20, only SPPs can be excited and the influence of the filling factor is enhanced with an increase of the depth. When the ratio is between 1/20 and 1/2, the resonant wavelength of SPPs redshifts at first with the increase of the filling factor due to the increase of the effective refractive index. When the filling factor is increased to be larger than 0.7, the field between the two adjacent corners of the grating starts to be coupled. The air gap under excitation exhibits a similar resonance as in an air

*Project supported by the National Natural Science Foundation of China (Grant Nos. 61378082 and 61675070) and the Project of High-level Professionals in the Universities of Guangdong Province, China.

†Corresponding author. E-mail: ljwu@scnu.edu.cn

© 2017 Chinese Physical Society and IOP Publishing Ltd

rod,[19] which blue-shifts with the increase of the filling factor. When the ratio between the depth and the period is larger than 1/2, besides SPPs and air gap resonances, surface plasmon standing wave modes can be excited due to the formation of the waveguide of the grating wall–air–wall, which can be regarded as a metal–insulator–metal (MIM) structure. The influence of the geometric parameters on the thermal emission properties can not only provide us with direct information on how to choose appropriate parameters for thermal emission sources in different applications, but also help us understand the coupling mechanism between the incident electromagnetic waves and gratings with different parameters in various research fields.

2. Simulation model

The schematic of the grating is shown in Fig. 1, in which a, w, and h represent the period, width, and depth of the grating, respectively. We focus on discussing one-dimensional (1D) grating in this paper. The results would be meaningful references for two-dimensional (2D) grating although the confinements along two directions could influence each other, which is out of the discussion range of this paper. The filling factor is defined as $f = w/a$. Tungsten is chosen as the material because of its wide usage in thermal emissions.[8,20] Simulations are based on rigorous coupled wave analysis (RCWA, Rsoft) and finite element analysis (FEA, commercial COMSOL Multiphysics). RCWA is used to calculate the absorption spectra and FEA is used to find the electric field distributions. A perfectly matched layer (PML) boundary condition is applied for the top/bottom area and the periodic boundary condition (PBC) is used for the two walls. The grid size is chosen to be 10 nm to ensure the convergence of the simulation results. In the simulations, the dielectric constant of tungsten is related to the frequency of the incident light. This relationship is defined by the Drude model[21]

$$\varepsilon = 1 - \frac{\omega_{\mathrm{p}}^2}{\omega(\omega + \mathrm{i}\omega_{\mathrm{c}})}, \tag{1}$$

where $\omega_{\mathrm{p}} = 1.448 \times 10^{15}$ Hz and $\omega_{\mathrm{c}} = 1.3 \times 10^{13}$ Hz.

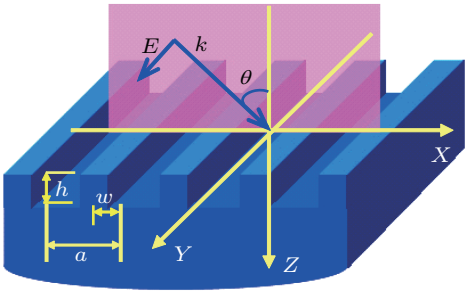


Fig. 1. (color online) Schematic of the simulated 1D tungsten grating. The geometry of the grating is defined by its period (a), width of the ridge (w), and groove depth (h).

In the simulations, the thickness of the substrate is set as 500 nm, which is much larger than the skin depth of tungsten (about 20 nm), thus no light can penetrate and $T(\lambda) = 0$. According to Kirchhoff's law, the spectral emissivity (at a wavelength of λ) $\varepsilon(\lambda)$ is equal to the spectral absorbance $A(\lambda)$ at thermal equilibrium. The absorptivity for each λ is given by $A(\lambda) = 1 - R(\lambda) - T(\lambda)$, where $R(\lambda)$ and $T(\lambda)$ are the reflectivity and transmittivity of the incident wave.[22,23] Therefore, the emissivity can be directly related to the reflectivity by $\varepsilon(\lambda) = A(\lambda) = 1 - R(\lambda)$. As the waves incident vertically from the top, the emission direction is the reverse of the incidence and their polarizations are identical. The plane of incidence is defined by the incidence and the surface normal.

For a flat air–material interface, the surface plasmon wavevector propagating along the x direction, $k_{\mathrm{sp},x}$, is determined by the dielectric constant of the metal (ε_{m}) and the wavevector in a vacuum (k_0)[24]

$$k_{\mathrm{sp},x} = k_0 \sqrt{\frac{\varepsilon_{\mathrm{m}}(\omega)}{1 + \varepsilon_{\mathrm{m}}(\omega)}}. \tag{2}$$

SPPs can be excited between the metal and air if a 1D grating is modulated in the x direction. The wavevector of SPP is then given by[10]

$$k_{\mathrm{sp},x} = k_{ox} \pm jK_x = k_0 \sin\theta \pm j\frac{2\pi}{a}, \tag{3}$$

where K_x denotes the grating vector perpendicular to the grating grooves. Integer j represents the diffraction order, while "+" and "−" signs correspond to $j > 0$ and $j < 0$, respectively. θ is the resonant angle of the incidence, as defined in Fig. 1(a). When the light incidents vertically on the grating, $\theta = 0°$. Without loss of generality, we fix $\theta = 0°$ in the whole paper. The dielectric constant of tungsten, $|\varepsilon_{\mathrm{w}}| \gg \varepsilon_0 = 1$ when $\lambda > 2$ μm.[20] When $\theta = 0°$, the resonant wavelength of SPP, λ_{res}, is given by

$$\lambda_{\mathrm{res}} = \pm\frac{a}{j}\sqrt{\frac{\varepsilon_{\mathrm{w}}(\omega)}{1 + \varepsilon_{\mathrm{w}}(\omega)}}. \tag{4}$$

Thus the resonant wavelength λ_{res} and the period a are correlated. Actually, the above equation is derived for a plane surface. It may not be applicable in the presence of a grating with the filling factor being within some range, in which the effective dielectric constant of tungsten, $\varepsilon_{\mathrm{w}}^{\mathrm{eff}}$, close to air may be changed. Therefore, the resonant wavelength may be more precisely defined as follows:[14]

$$\lambda_{\mathrm{res}} = \pm\frac{\Lambda}{j}\sqrt{\frac{\varepsilon_{\mathrm{w}}^{\mathrm{eff}}(\omega)}{1 + \varepsilon_{\mathrm{w}}^{\mathrm{eff}}(\omega)}}. \tag{5}$$

As the emittance for higher order mode ($j > 1$) is much lower than that from the first order ($j = 1$),[14] we will mainly concentrate on discussing the emission at $j = 1$ for SPPs in the rest of the paper.

3. Results and discussion

We choose the period of the tungsten grating a to be 4 μm to illustrate the influences of other geometric parameters on the thermal emission properties. Similar results could be obtained for other periods. The grating depth h is divided into three ranges based on its relationship with the period: $h/a \leq 1/20$, $1/20 < h/a < 1/2$, and $h/a \geq 1/2$.

3.1. $h/a \leq 1/20$

When $h/a \leq 1/20$, the grating is very shallow. The bulge part (ridge) of the grating can be regarded as a perturbation although it affords the extra wavevector to excite SPPs. We choose $h = 0.1$ μm and 0.2 μm as two examples to examine the influence of the filling factor. Figure 2 shows the emission spectra with different filling factors (left panel) and the corresponding field distributions at resonant wavelengths (right panel). The arrows on the field map point to the vector direction of the electric field. As can be seen in Figs. 2(a) and 2(d), the emission peak approximately equals to the grating period $a = 4.0$ μm. This is consistent with the results shown in Ref. [13]. On the other hand, the position of the resonance peak exhibits very small variations with the filling factor. This is because f can affect the effective dielectric constant of the grating system and thus the resonant wavelength (refer to Eq. (6)). Meanwhile, the absorption, i.e., the emission of the material, is related with f since it can influence the ability to localize the field, as has been addressed in our previous paper.[14]

From the right panel field map, it can be seen that the electric field is localized close to the grating interface (air side) and attenuates away from the interface at resonance. All the vertical white dashed lines drawn in the field maps are guides for eye and arranged with equal transverse distance. We can observe that along the direction parallel to the grating plane, the field intensity located at each vertical white dashed line is similar. The periodicity of the field intensity distribution suggests the excitation of the propagating SPPs.

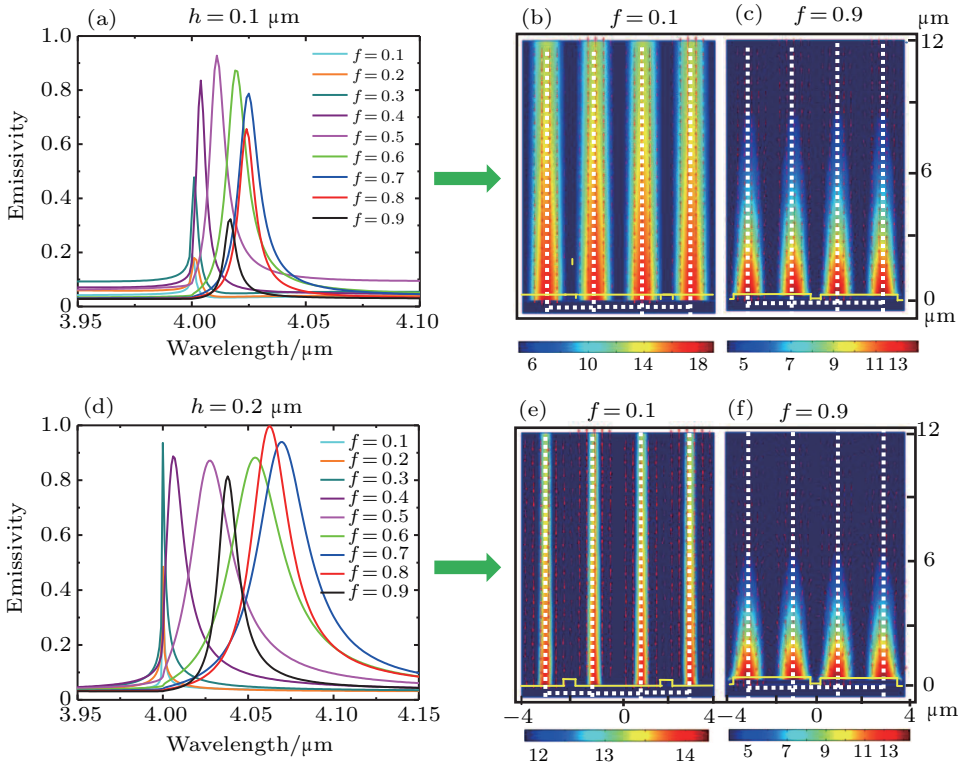


Fig. 2. (color online) Emissivity spectra at different filling factors for (a) $h = 0.1$ μm and (d) $h = 0.2$ μm. The corresponding field intensity distributions at resonances are plotted in panels (b), (c), (e), and (f). In each field map, the vertical white dashed lines are guides for the eye and arranged with equal transverse space (same in the whole paper). For SPPs, the field intensity is distributed periodically and the white vertical lines can label its periodicity.

3.2. $1/20 < h/a < 1/2$

When h/a is in the range from 1/20 to 1/2, the grooves of the grating can be regarded as cavities.[5,25,26] We choose the grating depth $h = 0.3$ μm, 0.6 μm, 1.0 μm, and 1.6 μm as examples to analyze the influence of the filling factor. A series of emission spectra with different filling factors and grating depths are plotted in Fig. 3. The details around the wavelength of 4 μm are shown in the left column. There are two types of resonant peaks in this range. We name the narrow one as resonance A and the wider one resonance B. As shown, the peak position of resonance A is fixed at 4 μm for all filling factors and grating depths. Its emission increases gradually with f

(in the range of 0.1–0.3) for $h \leq 1$ μm. It almost disappears when h is increased to be larger than 1 μm except for $f = 0.9$. For resonance B, however, the evolution of the peak with the geometrical parameters is different. With an increase of f, its peak position is first red-shifted and the shape is broadened simultaneously. After the turnoff point at $f = 0.7$, it is then blue-shifted and narrowed. When $h > 1$ μm and $f < 0.6$, both resonances A and B are weak and they appear again for $f > 0.7$. The shift of the peak becomes insensitive to f in this case. With a further increase of h, resonance B keeps redshift, although its position is almost not related with f. When h is increased to be larger than 1.6 μm, another resonant peak at 4 μm appears for $f = 0.9$. We are investigating the underlying mechanism of these resonant peaks by plotting the corresponding field distributions in the following.

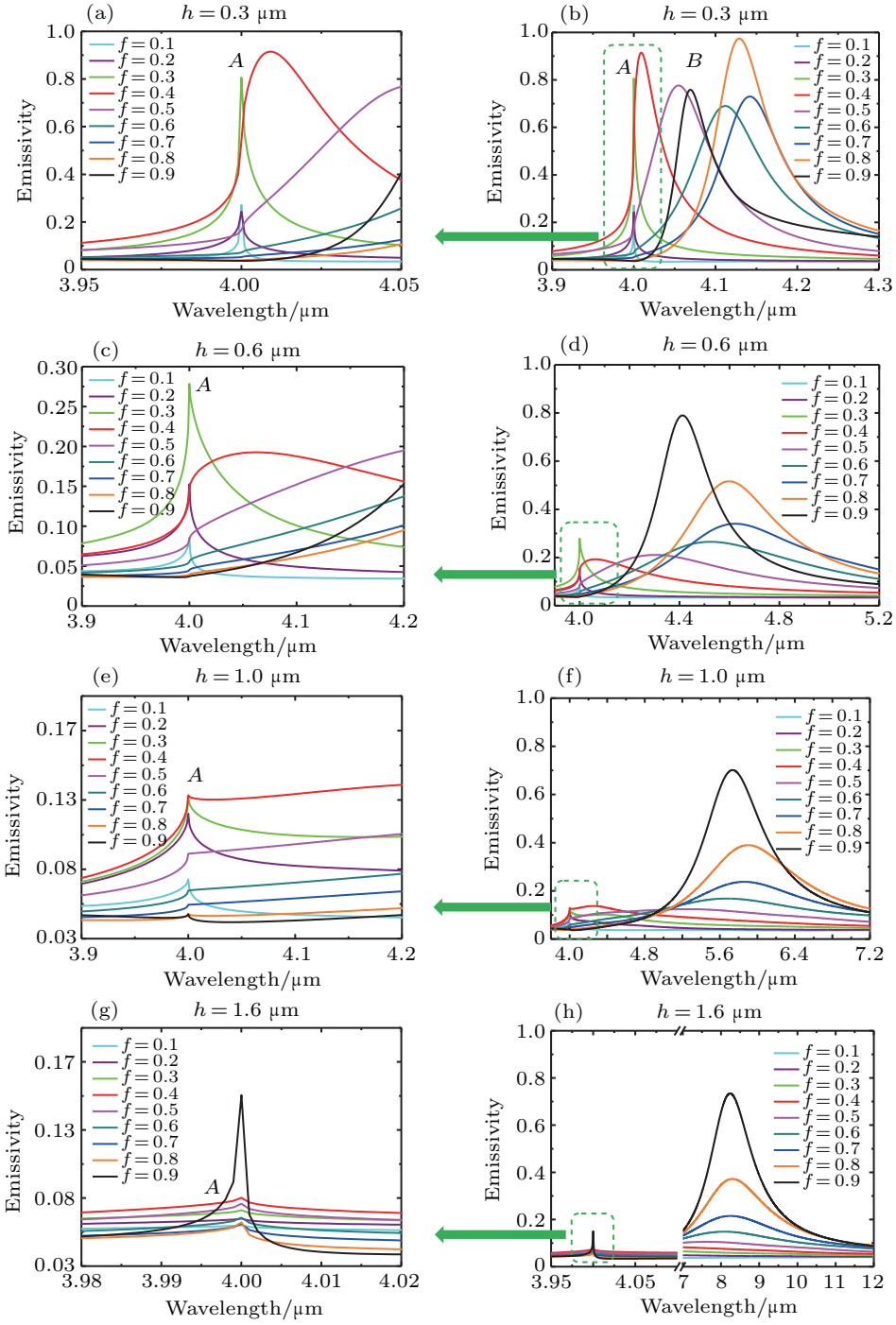


Fig. 3. (color online) Emissivity spectra of the grating at different filling factors with (a), (b) $h = 0.3$ μm, (c), (d) $h = 0.6$ μm, (e), (f) $h = 1.0$ μm, and (g), (h) $h = 1.6$ μm. Resonance A represents the peak that is narrow and fixed at 4 μm, while resonance B is wide and varied (same as Fig. 4). The details of the emission spectra at around 4 μm are demonstrated in the left column.

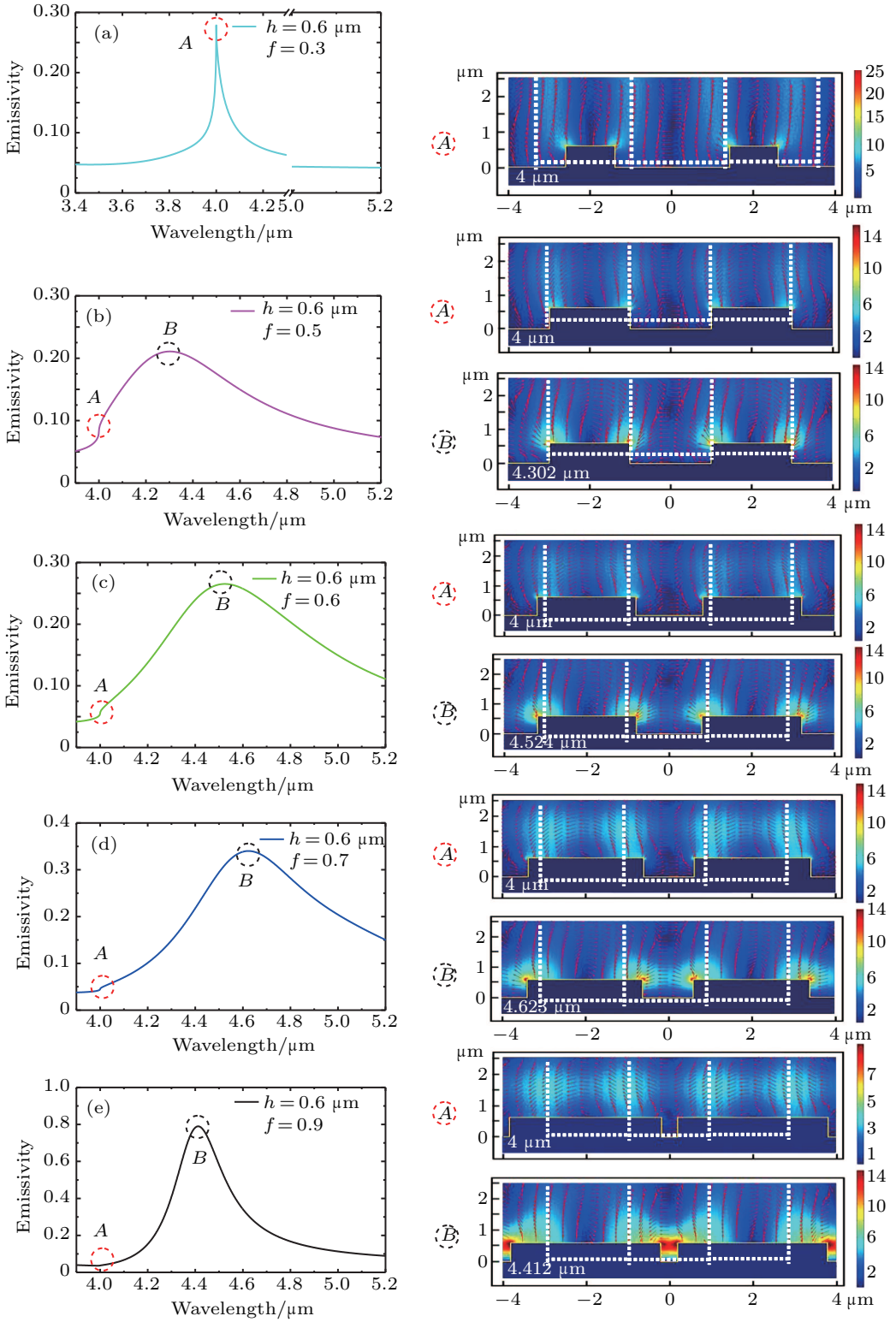


Fig. 4. (color online) Emissivity spectra (left column) and the corresponding field intensity distributions (right column) at different filling factors for $h = 0.6$ μm.

Firstly, we select the geometric parameters $h = 0.6$ μm and $f = 0.3$, 0.5, 0.6, 0.7, 0.9. As can be seen in Fig. 4, the radiation resonant peak of resonance A is narrow for $f = 0.3$. The corresponding field distribution in the right column shows obvious SPP characteristics, which is similar to the results shown in Fig. 2. When f is increased to be larger than 0.5, the resonant peak is being gradually widened. By zooming in the radiation spectrum near 4.0 μm, we can see a saltation at the wavelength of 4.0 μm for all the filling factors. From the corresponding field distribution, it can be seen that the surface electric field is localized near the grating surface and always exhibits SPP characteristics although the intensity is different. For $1/20 < h/a < 1/2$, the ridge of the grating can affect the field distribution significantly, which is different from the shal-

low grating ($h/a < 1/20$) demonstrated in Fig. 2.

When $f < 0.5$, the interaction between the two corners of the same ridge is dominant. Under this situation, the ridge can be approximated as a metallic nanorod. With an increase of the filling factor, the ridge is widened and the aspect ratio of the nanorod is increased. Thus the resonant wavelength is red-shifted due to the increased retardation.[27] For $f > 0.5$, the interaction between the two adjacent corners across the air gap starts to appear and becomes dominant gradually. From the field intensity map shown in Fig. 4(c), we can see that the field is localized around the ridge corner and they attract each other. The field intensity decays faster away from the grating interface than at 4 μm. When $f = 0.7$, the attraction is strengthened, inducing a non-uniform distribution of the field along the grating plane. This can be observed in the right column of Figs. 4(d) and 4(e), in which the distribution of the equi-field-intensity deviates from the vertical white dashed lines (arrayed with equi-transverse-distance). The obvious difference of the field distribution from resonance *A* suggests that resonance *B* does not exhibit the SPP feature. Further increasing f can enhance the attraction and cause the coupling resonance between the two adjacent corners across the air gap to become dominant. In this case, the air gap can be approximated as an air rod[19] and the incident wave parallel to the grating plane can excite its resonant mode. A narrower air gap corresponds to a smaller dipole momentum, which induces an increase of the vibration frequency.[18] Therefore, the resonance peak is blue-shifted as shown in Figs. 3(a)–3(d).

As has been pointed out in Figs. 3(g) and 3(h), besides the enhanced broad resonance mode, an obvious narrow resonance mode at 4.0 μm re-appears when f is increased to 0.9 under $h = 1.6$ μm. We draw the electric field intensity distributions of the broad and narrow resonances in Fig. 5. At the wavelength of 8.24 μm, we can find that the electric field intensity is localized at the corners of the grating, similar to that described in the above context. For the narrow resonant mode at the wavelength of 4.0 μm, the electric field intensity is localized not only on the grating surface showing the SPP characteristic but also inside the air gap. Therefore, the two resonant modes are superimposed at around 4.0 μm, which will be addressed in the following context.

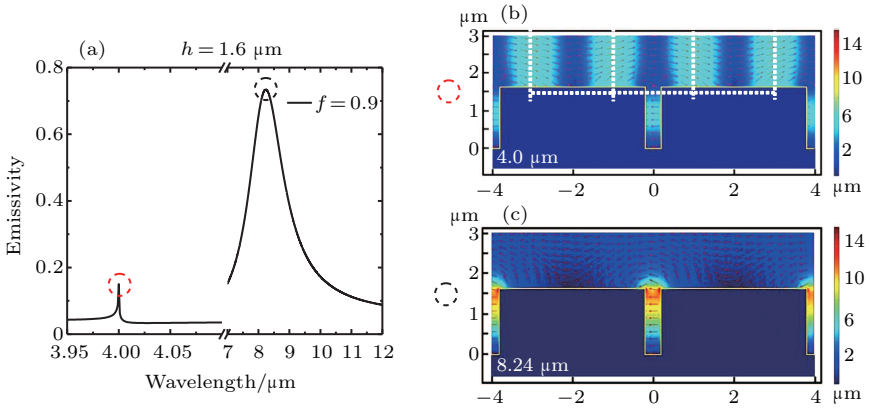


Fig. 5. (color online) (a) Emissivity spectrum for the grating with $h = 1.6$ μm and $f = 0.9$. The corresponding field intensity distributions at the wavelengths of (b) 4 μm and (c) 8.24 μm.

3.3. $h/a \geq 1/2$

When the grating depth h is larger than half of the period (here $h \geq 2$ μm), it can be defined as deep grating.[28] Due to the large depth, the two walls of the air gap on the grating can form a metal–insulator–metal (MIM) structure,[29] in which the wave-front and wave-end of the traveling wave can interfere and form surface plasmon standing wave (SPSW) modes.[28,30–33] The SPSW can localize energy inside the air gap and enhance the absorption and thus the emission of the grating. With an increase of f, the coupling between the two walls can be strengthened and lead to stronger emission.

To identify the order of the SPSW modes, we choose the depth of the grating to be as high as 6.0 μm in order to illustrate the antinodes and nodal points of the standing wave modes obviously. Figure 6 illustrates the emission spectrum and the corresponding field intensity distributions at different resonances with $f = 0.7$, in which white circles mark the nodal points. As can be seen, there are three distinct resonance peaks in the emission spectrum. From the field intensity maps, obvious standing waves corresponding to different orders can be observed inside the air gap of the grating. The resonant wavelength of the standing wave (λ_{sw}) is given by[34]

$$\lambda_{sw} = \frac{2}{m} h_n, \tag{6}$$

where h_n is the distance between two nodal points and m is the ordinal number of the nodal points within h_n (starting from zero). The field intensity maps in Fig. 6(b) show that there are two nodal points, thus the SPSW mode is the first order ($i = 1$). As h_n is measured to be 4.4 μm, λ_{sw} can be calculated to be 8.8 μm, which is consistent with the value obtained in Fig. 6(a). Similarly, for the second and the third orders, i.e., $i = 2$ and $i = 3$, λ_{sw} can be calculated to be 5.3 μm and 4.0 μm from Figs. 6(c) and 6(d), respectively. The field intensity distribution for $i = 3$ shown in Fig. 6(d) seems different from that for $i = 1$ and $i = 2$. This is because the wavelength is close to the SPP resonance ($j = 1$). At this point, SPP and SPSW resonances can be observed simultaneously.

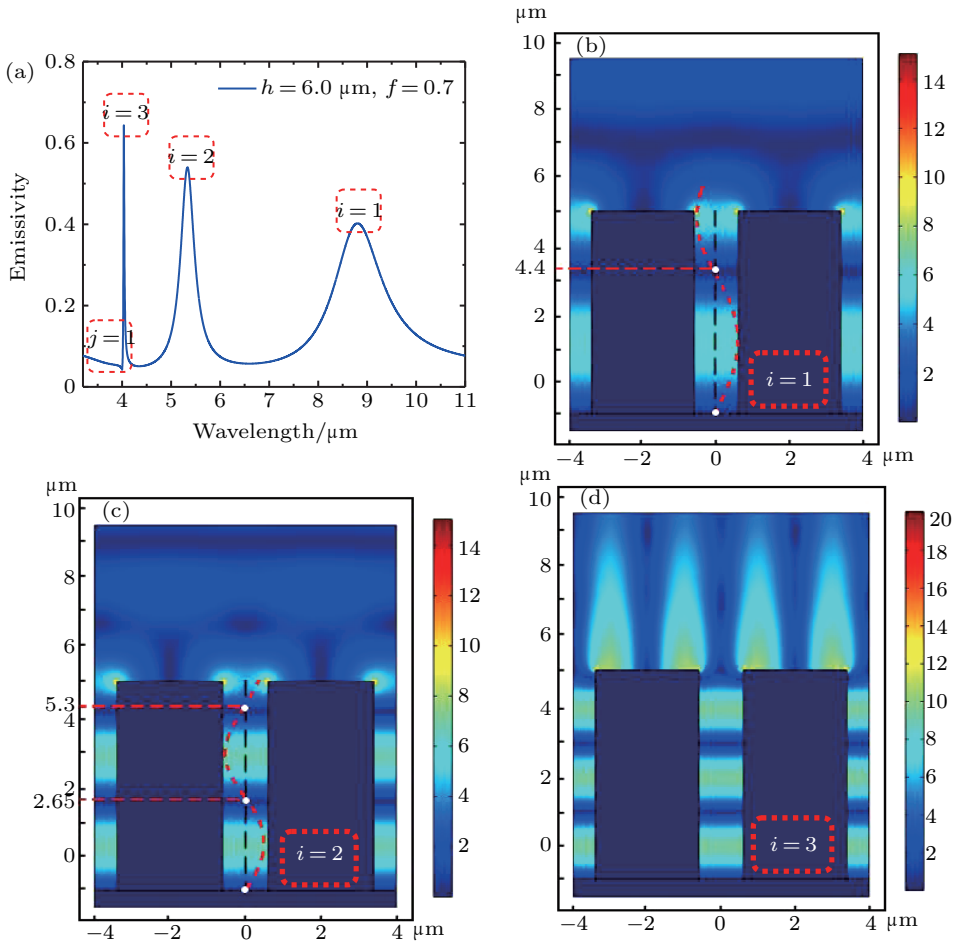


Fig. 6. (color online) (a) Emissivity spectrum for the grating with $h = 6.0$ μm and $f = 0.7$. $i = 1, 2, 3$ corresponds to the 1st, 2nd, and 3rd order of the SPSW mode. $j = 1$ represents the 1st order of the SPP resonance. The field intensity distributions are shown: (b) for $i = 1$, (c) for $i = 2$, and (d) for $i = 3$. The white circles mark the positions of the nodal points.

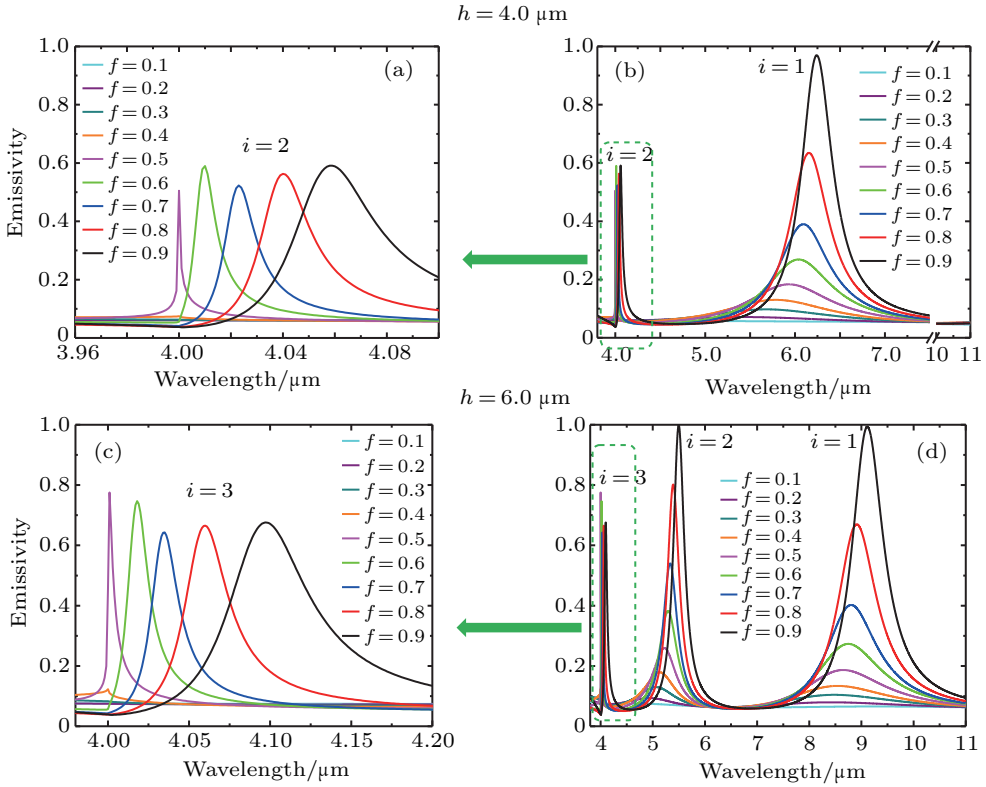


Fig. 7. (color online) Emissivity spectra at various filling factors for (a), (b) $h = 4.0$ μm and (c), (d) $h = 6.0$ μm. Panles (a) and (c) show the enlarged part of panels (b) and (d) at around 4 μm.

The wavelength of the SPSW resonance is closely related to the depth of the grating h and the filling factor f. As shown in Fig. 7, the SPSW resonance of the same order red-shifts when h is increased from 4.0 μm to 6.0 μm. Increasing f exhibits a similar trend while the resonance of the lower-order mode shifts faster. If $f \leq 0.4$, the field coupling between the adjacent corners across the air gap of the grating becomes very weak, thus SPSW modes are difficult to be excited. The corresponding emission curves are almost flat within the whole monitored wavelength range. Moreover, unlike the low-order mode, the intensity of the SPSW mode close to 4 μm is not very sensitive to f due to the influence of the SPP mode.

4. Conclusion

We studied the influence of the geometric parameters of the tungsten grating on its thermal emission properties. It was found that when the ratio between the depth and the period is smaller than 1/20, only SPP modes can be excited. The emission intensity is related with the filling factor. By increasing the grating depth, besides the SPP resonance, the field between adjacent corners can be coupled across the air gap of the grating when the filling factor is larger than 0.5. Further increase of the grating depth can induce surface plasmon standing wave modes because of the formation of the metal–insulator–metal structure when the filling factor is larger than 0.5. Our investigations will help understanding the mechanism of the geometric parameters affecting the emission properties of the periodic structures. Multiple resonances occurring on the tungsten grating can afford a platform to manipulate the thermal emission properties and thus offer the possibility to choose appropriate thermal emission sources according to applications. Furthermore, as the emission from the metallic grating is consistent with the absorption, our conclusions are applicable to photovoltaic and photoelectronic conversion applications.

References

[1] Porto J A, Garcia-Vidal F J and Pendry J B 1999 *Phys. Rev. Lett.* **83** 2845

[2] Shao L, Ruan Q F, Wang J F and Lin H Q 2014 *Physics* **43** 290

[3] Martin-Moreno L, García-Vidal F J, Lezec H J, Pellerin K M, Thio T, Pendry J B and Ebbesen T W 2001 *Phys. Rev. Lett.* **86** 1114

[4] Tong L M and Xu H X 2012 *Physics* **41** 582

[5] Barnes W L, Dereux A and Ebbesen T W 2003 *Nature* **424** 824

[6] Li X F, Peng W, Zhao Y L, Wang Q and Wei J L 2016 *Chin. Phys. B* **25** 37303

[7] Stockman I 2008 *Nat. Photon.* **2** 327

[8] Huang Z, Koschny Th and Soukoulis C M 2012 *Phy. Rev. Lett.* **108** 187402

[9] Sai H, Kanamori Y and Yugami H 2003 *Appl. Phys. Lett.* **82** 1685

[10] Greffet J J 2011 *Nature* **478** 191

[11] Laroche M, Arnold C, Marquier F, Carminati R, Greffet J J, Collin S, Bardou N and Pelouard J L 2005 *Opt. Lett.* **30** 2623

[12] Huu N N, Chen Y B and Lo Y L 2012 *Opt. Express* **20** 5882

[13] Chen Y B and Zhang Z M 2007 *Opt. Commun.* **269** 411

[14] Han F, Sun X L, Wu L J and Li Q 2013 *Opt. Express* **21** 28570

[15] Arnold C, Marquier F, Garin M, Pardo F, Collin S, Bardou N, Pelouard J L and Greffet J J 2012 *Phys. Rev. B* **86** 035316

[16] Maruyama S, Kashiwa T, Yugami H and Esashi M 2001 *Appl. Phys. Lett.* **79** 1393

[17] Hesketh P J, Zemel J N and Gebhart B 1986 *Nature* **324** 549

[18] Sobnack M B, Tan W C, Wanstall N P, Preist T W and Sambles J R 1998 *Phys. Rev. Lett.* **80** 5667

[19] Klein Koerkamp K J, Enoch S, Segerink F B, van Hulst N F and Kuipers L 2004 *Phys. Rev. Lett.* **92** 183901

[20] Rephaeli E and Fan S 2008 *Appl. Phys. Lett.* **92** 211107

[21] Rakić A D, Djurišić A B, Elazar J M and Majewski M L 1998 *Appl. Opt.* **37** 5271

[22] Hao J M, Zhou L and Qiu M 2011 *Phys. Rev. B* **83** 165107

[23] Fleming J G, Lin S Y, El-Kady I, Biswas R and Ho K M 2002 *Nature* **417** 52

[24] Raether H 2007 *Surface Plasmons* (Berlin:Springer)

[25] Arthur R D, Vyacheslav V P and Sergei A N 2012 *Phys. Rev. Lett.* **108** 127401

[26] Evgeny P, Nicolas B and Stefan E 2007 *Opt. Express* **15** 4224

[27] Rao W Y, Li Q, Wang Y Z, Li T and Wu L J 2015 *Acs Nano* **9** 2783

[28] Sai H, Kanamori Y, Hane K and Yugami H 2005 *J. Opt. Soc. Am. A* **9** 1805

[29] Zhou J and Guo L J 2014 *Sci. Rep.* **4** 3614

[30] Barnes W L, Preist T W, Kitson S C and Sambles J R 1996 *Phys. Rev. B* **54** 6227

[31] Barnes W L, Kitson S C, Preist T W and Sambles J R 1997 *J. Opt. Soc. Am. A* **7** 1654

[32] Félidj N, Aubard J, Lévi G, Krenn J R, Schider G, Leitner A and Aussenegg F R 2002 *Phys. Rev. B* **66** 245407

[33] Heinzel A, Boerner V, Gombert A, Bläsi B, Wittwer V and Luther J 2000 *J. Mod. Opt.* **13** 2399

[34] Chew W C 1995 *Waves and Fields in Inhomogeneous Media* (New York: Wiley-IEEE)